International Journal of Innovative Computing, Information and Control
Volume **18**, Number **6**, December **2022**

ICIC International ©2022 ISSN 1349-4198
pp. 1769–1784

A NEW MODEL FOR THE COMPLETE DESIGN OF CIRCULAR ISOLATED FOOTINGS CONSIDERING THAT THE CONTACT SURFACE WORKS PARTIALLY UNDER COMPRESSION

David Samuel Kim-Sánchez[1], Arnulfo Luévanos-Rojas[1,*]
José Daniel Barquero-Cabrero[2], Sandra López-Chavarría[1]
Manuel Medina-Elizondo[1] and Inocencio Luévanos-Soto[3]

[1]Instituto de Investigaciones Multidisciplinaria
Facultad de Contaduría y Administración
Universidad Autónoma de Coahuila, Unidad Torreón
Blvd. Revolución 151 Ote. CP 27000, Torreón, Coahuila, México
{ dkim; salopezc; mamedinae }@uadec.edu.mx
*Corresponding author: arnulfoluevanos@uadec.edu.mx

[2]Institute for Long Life Learning (IL3)
University of Barcelona
Street Girona No. 24, CP 08010, Barcelona, Spain
jd.barquero@eserp.com

[3]Facultad de Ingeniería, Ciencias y Arquitectura
Universidad Juarez del Estado de Durango, Unidad Gómez Palacio
Av. Universidad S/N, Fracc. Filadelfia, CP 35010, Gómez Palacio, Durango, México
inocencio.luevanos@ujed.mx

Received May 2022; revised August 2022

Abstract. *This paper presents a new model for the complete design of circular isolated footings considering that the contact surface works partially under compression. The writers used the footing contact surface equations described earlier in a companion paper. The methodology is developed by integration to obtain the moments, the bending shear and the punching shear by means of the pressure volume below of the footing. Other authors present the equations to obtain the design for the circular isolated footing, but consider the total area working under compression. Also, a comparison is presented between the new model (contact surface works partially to compression) and the model proposed by other authors (contact surface works totally to compression). Therefore, the new model is more economic with respect to the model proposed by other authors.*
Keywords: Circular isolated footings, Complete design, Moments, Bending shear, Punching shear

1. Introduction.

Design of shallow foundations dependent on the application of the loads can be: 1) the footings under concentric load; 2) the footings under uniaxial bending; 3) the footings under biaxial bending [1,2].

Figure 1 presents the distribution of soil pressure under the footing according to the stiffness of the footing and the type of soil. Figure 1(a) shows a rigid footing on sandy soil. Figure 1(b) presents a rigid footing on clay soil. Figure 1(c) shows a flexible footing on sandy soil. Figure 1(d) presents a flexible footing on clay soil. Figure 1(e) shows the uniform distribution used in the current design [1].

The pressure distribution diagrams can be applied when the center of gravity of the footing coincides with the position of the resultant force (see Figure 1).

DOI: 10.24507/ijicic.18.06.1769

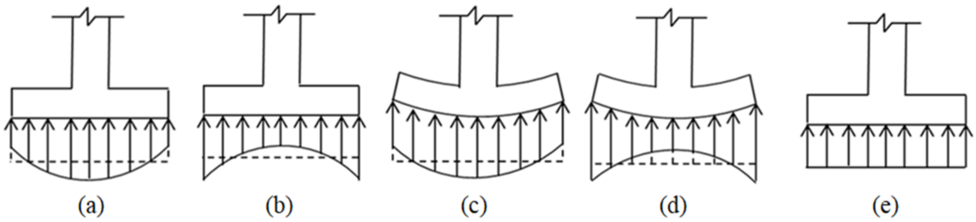

Figure 1. Distribution of the soil pressure under footing

The works which present the dimensions of the contact surface on the soil for foundations are: for square, rectangular and circular isolated footings [3-9]; for strap, trapezoidal, rectangular, corner and T-shaped combined footings [10-15]. These models consider the entire contact surface working in compression.

Other researchers have presented mathematical models to obtain the stresses at the base of rectangular isolated footings that consider a linear distribution of soil pressure and the contact surface working partially in compression [16-23].

The analytical models have been studied by several researchers to obtain the design of isolated footings subjected to an axial load and two moments on the X and Y axes (biaxial bending) and taking into account the linear distribution of the soil for rectangular isolated footings by Luévanos-Rojas et al. [24], for circular isolated footings by Luévanos-Rojas [25], for square isolated footings by López-Chavarría et al. [26]. Other researchers have developed mathematical models to obtain the design of combined footings subjected to an axial load and two moments in orthogonal directions (biaxial bending) in each column and taking into account the linear distribution of the soil for boundary rectangular combined footings by Luévanos-Rojas [27], for rectangular combined boundary footings with two restricted opposite sides by Luévanos-Rojas [28], for boundary trapezoidal combined footings by Luévanos-Rojas [29], for T-shaped combined footings by Luévanos-Rojas et al. [30], for strap combined footings by Yáñez-Palafox et al. [31]. Also, several researchers have presented optimal models for the design of isolated footings under the criterion of minimum cost for rectangular isolated footings by Luévanos-Rojas et al. [32], and for circular isolated footings by López-Chavarría et al. [33]. Also, these models consider the entire contact surface working in compression.

According to the bibliographic review, the closest papers are the new design and optimal model of circular isolated footings, but the contact surface with the soil woks totally under compression. Therefore, there is no paper with the current level of knowledge about the design of circular isolated footings considering that contact surface works partially in compression.

This paper shows an analytical model to obtain the complete design to obtain the thickness and areas of longitudinal and transverse steel of the circular isolated footings considering that contact area with the soil works partially to compression on the basis that the contact area with the soil proposed by Soto-García et al. [34], and the methodology is developed by integration to obtain the pressure volume below footing. Other authors present the equations to obtain the design for the circular isolated footing, but consider the total area working under compression. Also, a comparison is presented between the new model (contact surface works partially to compression) and the model proposed by other authors (contact surface works totally to compression) to observe the differences between the two models. In addition, this study presents the characteristics of the environment indicator related to quality of life [35].

The paper is organized as follows. Section 2 describes the methodology according to the building code requirements for structural concrete (ACI 318-19) [36]. Subsection 2.1 shows the formulation of the new model assuming that the contact surface works partially to compression. Subsection 2.2 presents the equations of the model proposed by Luévanos-Rojas (contact surface works totally to compression) [25]. Section 3 presents the numerical problems. Subsection 3.1 shows the numerical example for the new model. Subsection 3.2 presents the numerical example for the model proposed by Luévanos-Rojas [25]. Section 4 shows the results. Section 5 presents the conclusions to complete the paper.

2. **Methodology.** Building code requirements for structural concrete (ACI 318-19) mentions the following [36]:

1) For location of critical sections for moment, shear, and development of reinforcement in footings, it shall be permitted to treat circular or regular polygon-shaped concrete columns or pedestals as square members with the same area.

2) Maximum factored moment "M_u" shall be computed at face of column, pedestal, or wall, for footings supporting a concrete column, pedestal, or wall.

3) Location of critical section for bending shear shall be measured from face of column, pedestal, or wall to a distance "d" (effective deep), for footings supporting a column, pedestal, or wall.

4) Location of the critical section for the punching shear is in the perimeter "b_0" around the column at a distance "$d/2$" from face of column or pedestal.

Figures 1 and 2 show a circular isolated footing under axial load and moment in two orthogonal directions (biaxial bending) proposed by Soto-Garcia et al. [34].

The pressure anywhere of the contact surface for the circular isolated footing "$\sigma_{y'}$" is obtained by Equation (12) in function of σ_p (available permissible load capacity of the soil), R (radius of the circular footing), y' (axis where the maximum stress is located) and $y_0{}'$ (distance from the origin to the axis where the stresses are zero, measured along the Y' axis) proposed by Soto-Garcia et al. [34].

In this section the two models are shown, the model proposed in this work (The contact area of the footing with the soil works partially in compression) and the model proposed by Luévanos-Rojas [25] (The contact area of the footing with the soil works totally in compression).

2.1. **Formulation of the new model.** Figure 2 shows the axes for the critical sections where the moments are presented. The points P_1 and P_2 are located where the stresses

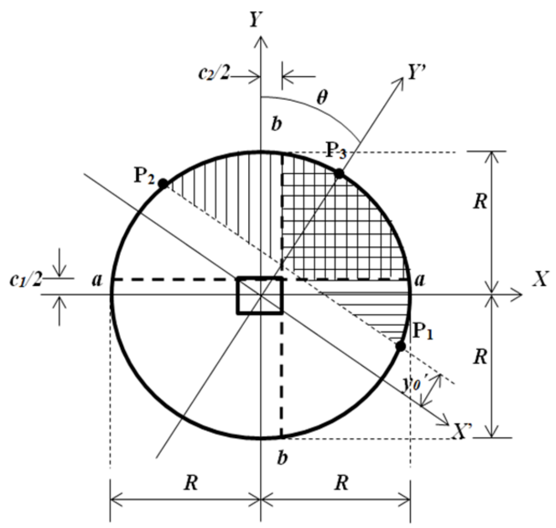

FIGURE 2. Critical sections for moments of a circular isolated footing

are zero, i.e., the line that joins the points P_1 and P_2 is the neutral axis and P_3 is located where the stress is maximum "σ_p". Here, "c_1" is the side of the column in the direction of the Y axis, "c_2" is the side of the column in the direction of the X axis, "θ" is the inclination angle of the Y' axis with respect to the Y axis, the X' and Y' axes are the rotated coordinates, the X and Y axes are the original coordinates.

Critical sections for moments appear in sections "*a-a*" and "*b-b*".

The general equation of a plane in 3-D is

$$Ax + By + C\sigma_z + D = 0 \tag{1}$$

The three known points of the plane in 3D are

$$\begin{gathered} P_1\left(\sqrt{R^2 - {y_0}'^2}\cos\theta + {y_0}'\sin\theta,\ {y_0}'\cos\theta - \sqrt{R^2 - {y_0}'^2}\sin\theta, 0\right) \\ P_2\left(-\sqrt{R^2 - {y_0}'^2}\cos\theta + {y_0}'\sin\theta, {y_0}'\cos\theta + \sqrt{R^2 - {y_0}'^2}\sin\theta, 0\right) \\ P_3\left(R\sin\theta, R\cos\theta, \sigma_p\right) \end{gathered} \tag{2}$$

Now, the general equation of the plane by determinant is obtained:

$$\begin{vmatrix} x - \sqrt{R^2 - {y_0}'^2}\cos\theta - {y_0}'\sin\theta & y + \sqrt{R^2 - {y_0}'^2}\sin\theta - {y_0}'\cos\theta & \sigma_z \\ -2\sqrt{R^2 - {y_0}'^2}\cos\theta & 2\sqrt{R^2 - {y_0}'^2}\sin\theta & 0 \\ (R - {y_0}')\sin\theta - \sqrt{R^2 - {y_0}'^2}\cos\theta & \sqrt{R^2 - {y_0}'^2}\sin\theta + (R - {y_0}')\cos\theta & \sigma_p \end{vmatrix} \tag{3}$$

The value of σ_z by Equation (3) is obtained:

$$\sigma_z = \frac{\sigma_p\left(y\cos\theta - {y_0}' + x\sin\theta\right)}{R - {y_0}'} \tag{4}$$

If it is required to find the equation of the straight line where the stresses are zero by Equation (4), it is obtained:

$$y\cos\theta - {y_0}' + x\sin\theta = 0 \tag{5}$$

The factorized moment on the "a" axis "M_{ua}" is obtained by the pressure "σ_z" and the area defined by the "a" axis, the equation of the straight line from the point P_2 to the "a" axis and the equation of the circumference, all this pressure is with respect to the "a" axis (see Figure 2).

The general equation of the factorized moment on the "a" axis "M_{ua}" is

$$\begin{aligned} M_{ua} = &\int_{{y_0}'\cos\theta + \sqrt{R^2 - {y_0}'^2}\sin\theta}^{R} \int_{-\sqrt{R^2-y^2}}^{\sqrt{R^2-y^2}} \sigma_z\left(y - \frac{c_1}{2}\right)dxdy \\ &+ \int_{\frac{c_1}{2}}^{{y_0}'\cos\theta + \sqrt{R^2 - {y_0}'^2}\sin\theta} \int_{\frac{{y_0}' - y\cos\theta}{\sin\theta}}^{\sqrt{R^2-y^2}} \sigma_z\left(y - \frac{c_1}{2}\right)dxdy \end{aligned} \tag{6}$$

The factorized moment on the "b" axis "M_{ub}" is obtained by the pressure "σ_z" and the area defined by the "b" axis, the equation of the straight line from the point P_1 to the "b" axis and the equation of the circumference, all this pressure is with respect to the "b" axis (see Figure 2).

The general equation of the factorized moment on the "b" axis "M_{ub}" is

$$M_{ub} = \int_{{y_0}'\sin\theta + \sqrt{R^2 - {y_0}'^2}\cos\theta}^{R} \int_{-\sqrt{R^2-x^2}}^{\sqrt{R^2-x^2}} \sigma_z\left(x - \frac{c_2}{2}\right)dydx$$

$$+\int_{\frac{c_2}{2}}^{y_0'\cos\theta+\sqrt{R^2-y_0'^2}\sin\theta}\int_{\frac{y_0'-x\sin\theta}{\cos\theta}}^{\sqrt{R^2-x^2}}\sigma_z\left(x-\frac{c_2}{2}\right)dydx \tag{7}$$

Figure 3 shows the axes of the critical sections where the bending shears occur. Critical sections for bending shears appear in sections "*c-c*" and "*e-e*".

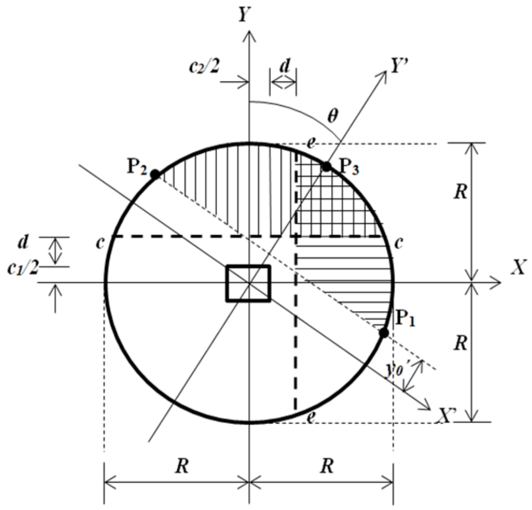

FIGURE 3. Critical sections for bending shears of a circular isolated footing

The factorized bending shear on the "c" axis "V_{uc}" is obtained by the pressure "σ_z" and the area defined by the "c" axis, the equation of the straight line from the point P_2 to the "c" axis and the equation of the circumference according to Figure 3.

The general equation of the factorized bending shear on the "c" axis "V_{uc}" is

$$\begin{aligned}V_{uc} &= \int_{y_0'\cos\theta+\sqrt{R^2-y_0'^2}\sin\theta}^{R}\int_{-\sqrt{R^2-y^2}}^{\sqrt{R^2-y^2}}\sigma_z dxdy \\ &\quad+\int_{\frac{c_1}{2}+d}^{y_0'\cos\theta+\sqrt{R^2-y_0'^2}\sin\theta}\int_{\frac{y_0'-y\cos\theta}{\sin\theta}}^{\sqrt{R^2-y^2}}\sigma_z dxdy\end{aligned} \tag{8}$$

The factorized bending shear on the "e" axis "V_{ue}" is obtained by the pressure "σ_z" and the area defined by the "e" axis, the equation of the straight line from the point P_1 to the "e" axis and the equation of the circumference according to Figure 3.

The general equation of the factorized bending shear on the "e" axis "V_{ue}" is

$$\begin{aligned}V_{ue} &= \int_{y_0'\sin\theta+\sqrt{R^2-y_0'^2}\cos\theta}^{R}\int_{-\sqrt{R^2-x^2}}^{\sqrt{R^2-x^2}}\sigma_z dydx \\ &\quad+\int_{\frac{c_2}{2}+d}^{y_0'\cos\theta+\sqrt{R^2-y_0'^2}\sin\theta}\int_{\frac{y_0'-x\sin\theta}{\cos\theta}}^{\sqrt{R^2-x^2}}\sigma_z dydx\end{aligned} \tag{9}$$

Figure 4 shows the perimeter of the critical section where the punching shear occurs. Critical sections for punching shear appear on the dotted line.

The factorized punching shear "V_{up}" is obtained by factorized axial load "P_u" of the column subtracting the pressure "σ_z" shown and the area defined in the Y direction of $-c_1/2-d/2$ to $c_1/2+d/2$ and in the X direction of $-c_2/2-d/2$ to $c_2/2+d/2$ according to Figure 4.

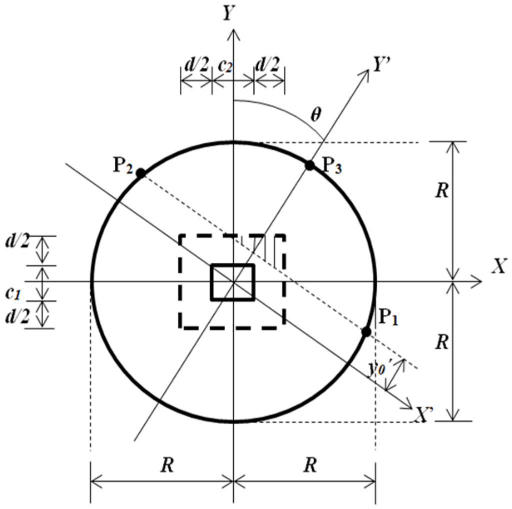

FIGURE 4. Critical section for punching shear of a circular isolated footing

The general equation of the factorized punching shear on the perimeter of the critical section "V_{up}" is

$$V_{up} = P_u - \int_{-\frac{c_1}{2}-\frac{d}{2}}^{\frac{c_1}{2}+\frac{d}{2}} \int_{-\frac{c_2}{2}-\frac{d}{2}}^{\frac{c_2}{2}+\frac{d}{2}} \sigma_z dxdy \tag{10}$$

2.2. **Equations of the model proposed by Luévanos-Rojas.** Figure 5 shows the axes for the critical sections where the moments are presented.

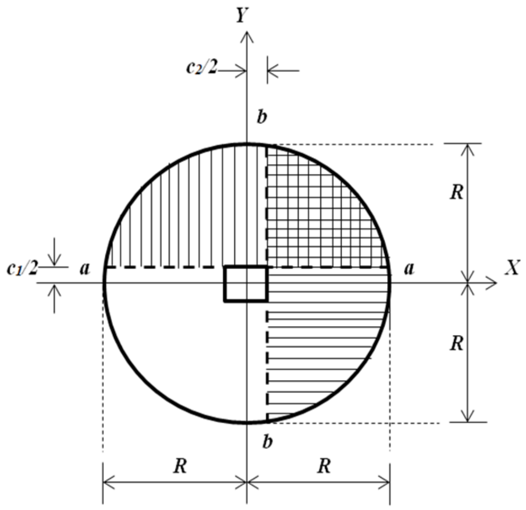

FIGURE 5. Critical sections for moments of a circular isolated footing

The general equation of the factorized moment on the "a" axis "M_{ua}" is [25]

$$\begin{aligned} M_{ua} = {} & \frac{(2M_{ux} - P_u c_1)}{4} + \frac{P_u \left(c_1^2 + 8R^2\right)\sqrt{4R^2 - c_1^2}}{24\pi R^2} \\ & + \frac{M_{ux} c_1 \left(c_1^2 - 10R^2\right)\sqrt{4R^2 - c_1^2}}{24\pi R^4} + \frac{(P_u c_1 - 2M_{ux})}{2\pi} \arcsin\left(\frac{c_1}{2R}\right) \end{aligned} \tag{11}$$

The general equation of the factorized moment on the "b" axis "M_{ub}" is [25]

$$M_{ub} = \frac{(2M_{uy} - P_u c_2)}{4} + \frac{P_u\left(c_2^2 + 8R^2\right)\sqrt{4R^2 - c_2^2}}{24\pi R^2} + \frac{M_{uy} c_2\left(c_2^2 - 10R^2\right)\sqrt{4R^2 - c_2^2}}{24\pi R^4} + \frac{(P_u c_2 - 2M_{uy})}{2\pi} \arcsin\left(\frac{c_2}{2R}\right) \tag{12}$$

Figure 6 shows the axes of the critical sections where the bending shears occur.

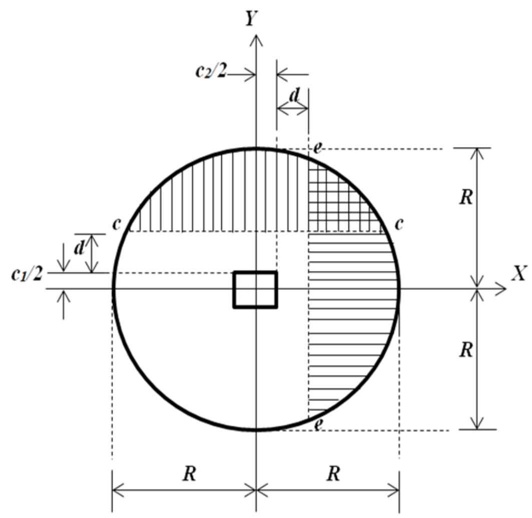

FIGURE 6. Critical sections for bending shears of a circular isolated footing

The general equation of the factorized bending shear on the "c" axis "V_{uc}" is [25]

$$V_{uc} = \frac{P_u}{2} - P_u\left(\frac{c_1 + 2d}{4\pi R^2}\right)\sqrt{4R^2 - (c_1 + 2d)^2} - \frac{P_u}{\pi}\arcsin\left(\frac{c_1 + 2d}{2R}\right) + \frac{M_{ux}\left[4R^2 - (c_1 + 2d)^2\right]^{3/2}}{3\pi R^4} \tag{13}$$

The general equation of the factorized bending shear on the "e" axis "V_{ue}" is [25]

$$V_{ue} = \frac{P_u}{2} - P_u\left(\frac{c_2 + 2d}{4\pi R^2}\right)\sqrt{4R^2 - (c_2 + 2d)^2} - \frac{P_u}{\pi}\arcsin\left(\frac{c_2 + 2d}{2R}\right) + \frac{M_{uy}\left[4R^2 - (c_2 + 2d)^2\right]^{3/2}}{3\pi R^4} \tag{14}$$

Figure 7 shows the perimeter of the critical section where the punching shear occurs.

The general equation of the factorized punching shear on the perimeter of the critical section "V_{up}" is [25]

$$V_{up} = P_u - \frac{P_u\,(c_1 + d)\,(c_2 + d)}{\pi R^2} \tag{15}$$

3. **Numerical Problems.** Three designs of circular isolated footings that support a square column are presented according to Figures 1 and 2 proposed by Soto-García et al. [34], and the following information is given: the column is of 40 × 40 cm; H (Depth of the footing) = 1.50 m; P_D (Dead load) = 300 kN (Example 1), 250 kN (Example 2) and 200 kN (Example 3); P_L (Live load) = 200 kN (Example 1), 150 kN (Example 2) and 100 kN (Example 3); M_{Dx} (Moment around the X axis of the dead load) = 200 kN-m; M_{Lx} (Moment around the X axis of the live load) = 100 kN-m; M_{Dy} (Moment around

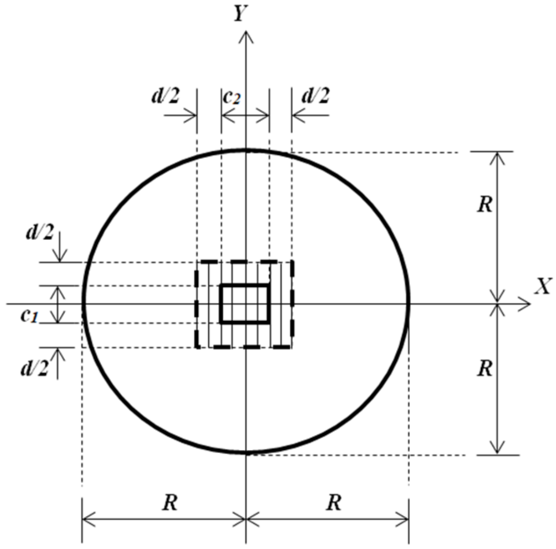

FIGURE 7. Critical section for punching shear of a circular isolated footing

the Y axis of the dead load) = 60 kN-m; M_{Ly} (Moment around the Y axis of the live load) = 40 kN-m; f'_c (Specified compressive strength of concrete at 28 days) = 21 MPa; f_y (Specified yield strength of steel reinforcement) = 420 MPa; q_a (Permissible load capacity of the soil) = 220 kN/m^2; γ_c (Concrete density) = 24 kN/m^3; γ_s (fill soil density) = 15 kN/m^3. The available permissible load capacity of the soil "σ_p" is obtained as follows: the permissible load capacity of the soil "q_a" is subtracted from the weight of the footing "γ_{ppz}" (γ_c by the thickness of the footing), and the weight of the soil fill "γ_{pps}" (γ_s by the thickness of the soil fill).

3.1. **New model.** The thickness of the footing must satisfy the moments, bending shear, and punching shear. After making several proposals for the three examples, the thickness that meets the conditions mentioned above is 30 cm. Therefore, the available permissible load capacity of the soil is $\sigma_p = 194.80$ kN/m^2.

Substituting M_y and M_x into Equation (2) proposed by Soto-García et al. [34], and the resultant moment for the three examples is obtained: $M_R = 316.23$ kN-m. Now, substituting P and M_R into Equation (6) proposed by Soto-García et al. [34], and the eccentricity is found: $e_R = 63.25$ cm (Example 1), 79.06 cm (Example 2) and 105.41 cm (Example 3). By Equation (10) proposed by Soto-García et al. [34], it is obtained: $R =$ 1.49 m (Example 1), 1.44 m (Example 2) and 1.40 m (Example 3). Then $e_R > R/4$ for the three examples (resultant force is located outside the central nucleus of the footing). Substituting σ_p, P and M_R into Equations (17) and (20) proposed by Soto-García et al. [34] are obtained: R and y_0'. Therefore, the proposed radius of the footings will be $R =$ 1.55 m (Example 1), 1.55 m (Example 2) and 1.70 m (Example 3). Now, substituting R, P and M_R into Equations (17) and (20) proposed by Soto-García et al. [34] are obtained: $\sigma_{\max}$ (maximum stress acting) and y_0'.

The factored mechanical elements (P_u, M_{ux} and M_{uy}) that act on the footing are obtained by $P_u = 1.2P_D + 1.6P_L$, $M_{ux} = 1.2M_{Dx} + 1.6M_{Lx}$ and $M_{uy} = 1.2M_{Dy} + 1.6M_{Ly}$.

The inclination angle of the Y' axis with respect to the Y axis by Equation (3) proposed by Soto-García et al. [34] is obtained: $\theta = 0.33$ Radians (for the three examples).

The factored resultant moment by Equation (2) proposed by Soto-García et al. [34] is obtained: $M_{uR} = 422.49$ kN-m (for the three examples).

Now, substitute R, P_u and M_{uR} into Equations (17) and (20) proposed by Soto-García et al. [34] to find the values of σ_{up} (ultimate design stress) and y_0' (for the three examples).

Table 1 shows all the values of the three examples of circular isolated footings obtained for the new model.

TABLE 1. New model

Example	R (m)	y_0' (m)	R (m)	$\sigma_{\max}$ (kN/m^2)	y_0' (m)	σ_{up} (kN/m^2)	y_0' (m)
	By Equations (17) and (20) [34]		Proposed	By Equations (17) and (20) [34]		By Equations (17) and (20) [34]	
1	1.53	−0.72	1.55	185.63	−0.76	248.19	−0.79
2	1.55	−0.32	1.55	194.19	−0.32	258.19	−0.34
3	1.65	0.20	1.70	174.32	0.14	142.48	−0.56

The moment "M_{ua}" on the "a" axis by Equation (6) and the moment "M_{ub}" on the "b" axis by Equation (7) are obtained.

The effective deep "d" is obtained by the code for each moment (ACI 318-19) [36]: d_a and d_b, the values of "d" are less than 22 cm for the three examples (minimum dimension according to the code), therefore, the proposed dimensions are: $d = 22$ cm, r (Cover over the reinforcing steel) $= 8$ cm and t (Total thickness) $= 30$ cm.

The bending shear "V_{uc}" on the "c" axis by Equation (8) and the bending shear "V_{ue}" on the "e" axis by Equation (9) are obtained. The bending shear resisted by concrete is (ACI 318-19) [36]: $\text{Ø}_v V_{cf}$. Therefore, V_{uc} and $V_{ue} \leq \text{Ø}_v V_{cf}$ must meet.

The punching shear "V_{up}" on critical perimeter by Equation (10) is obtained. The punching shear resisted by concrete are (ACI 318-19) [36]: $\text{Ø}_v V_{cp}$. Therefore, $V_{up} \leq \text{Ø}_v V_{cp}$, must meet.

The main reinforcing steel areas "A_{spy} and A_{spx}" in the X and Y axis directions, the minimum steel areas "A_{smin}" are obtained according to the code [36].

The minimum development length for deformed bars is found (ACI 318-14) [36]: L_d. The available length of the footing is L_a. Then, $L_d < L_a$. Therefore, it does not require a hook (for the three examples).

3.2. **Model proposed by Luévanos-Rojas.** The thickness of the footings and the resultant moments "M_R" are the same as in the new model.

Now, substituting P and M_R into Equations (9) and (10) presented by Soto-García et al. [34] are obtained the radius, and the eldest is the one who governs.

Therefore, the proposed radius of the footings will be $R = 2.55$ m (Example 1), 3.20 m (Example 2) and 4.25 m (Example 3).

Table 2 shows all the values of the three examples of circular isolated footings obtained for the model proposed by Luévanos-Rojas [4].

TABLE 2. Model proposed by Luévanos-Rojas [4]

Example	R (m)			$\sigma_{\max}$ (kN/m^2)	$\sigma_{\min}$ (kN/m^2)
	By Equation (9) [34]	By Equation (10) [34]	Proposed	By Equation (8) [34]	
1	2.53	1.49	2.55	48.76	0.19
2	3.16	1.44	3.20	24.72	0.15
3	4.22	1.40	4.25	10.53	0.04

The factored mechanical elements (P_u, M_{ux} and M_{uy}) are the same as in the new model.

The moment "M_{ua}" on the "a" axis by Equation (11) and the moment "M_{ub}" on the "b" axis by Equation (12) are obtained.

The effective deep "d" is the same as in the new model.

The bending shear "V_{uc}" on the "c" axis by Equation (13) and the bending shear "V_{ue}" on the "e" axis by Equation (14) are obtained. The bending shear resisted by concrete is (ACI 318-19) [36]: $Ø_v V_{cf}$. Therefore, V_{uc} and $V_{ue} \leq Ø_v V_{cf}$ must meet.

The punching shear "V_{up}" on critical perimeter by Equation (15) is obtained. The punching shear resisted by concrete are (ACI 318-19) [36]: $Ø_v V_{cp}$. Therefore, $V_{up} \leq Ø_v V_{cp}$, must meet.

The main reinforcing steel areas "A_{spy} and A_{spx}" in the X and Y axis directions, the minimum steel areas "A_{smin}" are obtained according to the code [36].

The minimum development length for deformed bars is found (ACI 318-14) [36]: L_d. The available length of the footing is L_a. Then, $L_d < L_a$. Therefore, it does not require a hook (for the three examples).

4. **Results.** Tables show the comparison of the two models for the three examples: The NM (new model) proposed in this document and the MPLR (model proposed by Luévanos-Rojas).

Table 3 presents the moments M_{ua} and M_{ub}, the analysis widths by bending b_{wb}, the bending shears that act V_{uc} and V_{ue}, the permissible bending shear $Ø_v V_{cf}$, the analysis widths for bending shear b_{ws}, the punching shear that acts V_{up}, the permissible punching shear $Ø_v V_{cp}$, the perimeter of the critical section for punching shear b_0 for the two models.

TABLE 3. Moments, bending shears and punching shears

Concept	Example 1			Example 2			Example 3		
	NM	MPLR	MPLR /NM	NM	MPLR	MPLR /NM	NM	MPLR	MPLR /NM
M_{ua} (kN-m)	328.79	476.81	1.45	312.43	493.66	1.58	242.81	505.99	2.08
M_{ub} (kN-m)	212.46	362.33	1.71	175.08	375.64	2.15	144.91	384.52	2.65
b_{wb} (m)	3.07	5.08	1.65	3.07	6.39	2.08	3.38	8.49	2.51
V_{uc} (kN)	411.58	401.80	0.98	400.60	330.92	0.83	285.67	254.69	0.89
V_{ue} (kN)	287.57	314.17	1.09	237.95	261.02	1.10	180.72	202.01	1.12
b_{ws} (m)	2.98	5.03	1.69	2.98	6.34	2.13	3.29	8.46	2.57
$Ø_v V_{cf}$ (kN)	434.13	732.82	1.69	434.13	923.61	2.13	479.29	1232.45	2.57
V_{up} (kN)	647.79	667.20	1.03	522.15	533.55	1.02	386.43	397.29	1.03
b_0 (m)	2.48	2.48	1.00	2.48	2.48	1.00	2.48	2.48	1.00
$Ø_v V_{cp}$ (kN)	1083.86	1083.86	1.00	1083.86	1083.86	1.00	1083.86	1083.86	1.00
	978.70	978.70	1.00	978.70	978.70	1.00	978.70	978.70	1.00
	701.32	701.32	1.00	701.32	701.32	1.00	701.32	701.32	1.00

Table 4 shows the reinforcing steel in the X and Y directions A_{spx} and A_{spy}, the minimum steel A_{smin}, the proposed reinforcing steel in the X and Y directions A_{sx} and A_{sy}, the rods spacing in the X and Y directions s_x and s_y of the two models.

Table 5 presents the radius R, the effective deep d, the cover over the reinforcing steel r, the total thickness t, the concrete volume V_C, the steel volume in the X and Y directions V_{Sx} and V_{Sy}, the total steel volume V_{St} for the two models.

Table 3 presents the following. The moments that act on the "a" and "b" axes are greater in the MPLR with respect to NM. The bending shear that acts on the "c" axis

TABLE 4. Reinforcing steel of the footings

Concept	Example 1			Example 2			Example 3		
	NM	MPLR	MPLR /NM	NM	MPLR	MPLR /NM	NM	MPLR	MPLR /NM
A_{spy} (cm^2)	42.71	61.29	1.44	40.41	62.65	1.55	30.69	63.38	2.06
A_{spx} (cm^2)	26.80	45.77	1.71	21.89	47.02	2.15	17.93	47.67	2.66
A_{smin} (cm^2)	22.54	37.28	1.65	22.54	46.86	2.08	24.79	62.26	2.51
A_{sy} (cm^2)	43.18 (34Ø1/2")	62.23 (49Ø1/2")	1.44	40.64 (32Ø1/2")	63.50 (50Ø1/2")	1.56	31.75 (25Ø1/2")	63.50 (50Ø1/2")	2.00
A_{sx} (cm^2)	27.94 (22Ø1/2")	46.99 (37Ø1/2")	1.68	22.86 (18Ø1/2")	48.26 (38Ø1/2")	2.11	25.40 (20Ø1/2")	63.50 (50Ø1/2")	2.50
s_y (cm)	9	10	1.11	9	12	1.33	14	17	1.21
s_x (cm)	14	14	1.00	17	17	1.00	17	17	1.00

TABLE 5. Volumes of the materials used to construct of footings

Concept	Example 1			Example 2			Example 3		
	NM	MPLR	MPLR /NM	NM	MPLR	MPLR /NM	NM	MPLR	MPLR /NM
R (cm)	155	255	1.65	155	320	2.06	170	4.25	2.50
d (cm)	22	22	1.00	22	22	1.00	22	22	1.00
r (cm)	8	8	1.00	8	8	1.00	8	8	1.00
t (cm)	30	30	1.00	30	30	1.00	30	30	1.00
V_C (m^3)	2.26	6.13	2.71	2.26	9.65	4.27	2.72	17.02	6.26
V_{Sy} (cm^3)	12644.05	30717.21	2.43	11900.28	39559.66	3.32	10250.33	52861.76	5.16
V_{Sx} (cm^3)	8134.50	23176.91	2.85	6624.28	30016.02	4.53	8131.89	52861.76	6.50
V_{St} (cm^3)	20456.18	54442.49	2.66	18524.56	69575.68	3.76	18382.22	105723.52	5.75

is greater in the NM with respect to MPLR, and the bending shear that acts on the "e" axis is greater in the MPLR with respect to NM. The punching shear that acts on the perimeter of the critical section is greater in the MPLR with respect to NM. This is for the three examples.

Table 4 shows the following. All reinforcing steel areas are larger for the MPLR with respect to the NM. This is for the three examples.

Table 5 presents the following. The radius, the volume of the concrete, the volume of the steel in the X and Y directions and the total volume of the steel are greater in the MPLR with respect to the NM. The effective deep, the cover over the reinforcing steel and the total thickness are the same. This is for the three examples.

Figure 8 shows the detailed diagram of a general shape of the circular isolated footing.

To verify the new model of this paper is as follows:

1) Replacing $c_1/2$ by $y_0' \cos\theta - \sqrt{R^2 - y_0'^2} \sin\theta$ and $y - c_1/2$ by y in Equation (6) gives: M_{ux} (Moment on the X axis), this moment is equal to the factored moment acting on the footing in the X axis.

2) Replacing $c_2/2$ by $y_0' \sin\theta - \sqrt{R^2 - y_0'^2} \cos\theta$ and $x - c_2/2$ by x in Equation (7) gives: M_{uy} (Moment on the Y axis), this moment is equal to the factored moment acting on the footing in the Y axis.

3) Replacing $c_1/2 + d$ by $y_0' \cos\theta - \sqrt{R^2 - y_0'^2} \sin\theta$ in Equation (8) gives: P_u, this load is equal to the factored axial load acting on the footing.

4) Replacing $c_2/2 + d$ by $y_0' \sin\theta - \sqrt{R^2 - y_0'^2} \cos\theta$ in Equation (9) gives: P_u, this load is equal to the factored axial load acting on the footing.

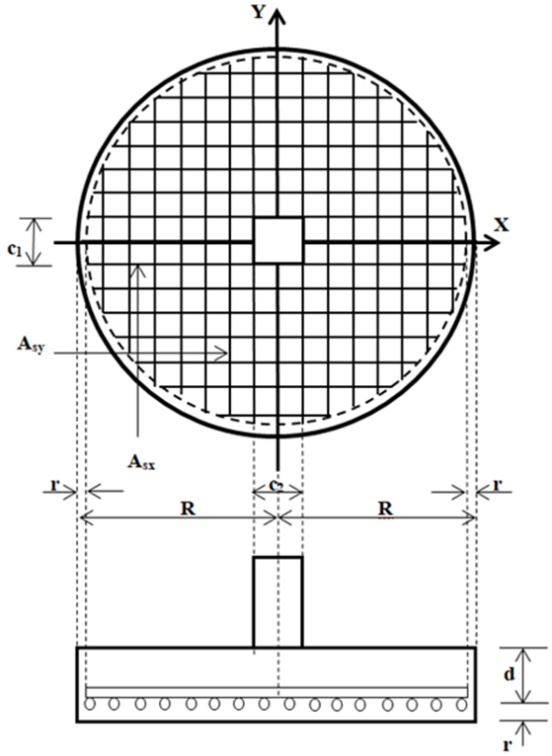

FIGURE 8. Diagram of the circular isolated footing

Therefore, the new model of this paper is verified, because it complies with the axial load and the moments applied due to the column against the soil pressure by Equations (6), (7), (8) and (9).

5. **Conclusions.** The new model presented in this paper applies only for design of circular isolated footings. This study presents a robust and effective solution applied only to obtaining the effective deep and the reinforcing steel of circular isolated footings resting on elastic soils, which satisfy with the linear distribution of the soil pressure.

The main contributions of this document are as the following.

1) The new model presents a significant reduction in the volumes of reinforcing steel and concrete, if the resultant force is located outside the central nucleus ($e_R > R/4$).

2) The thickness for the new model is governed by the bending shear, and for the model proposed by Luévanos-Rojas [25] it is governed by the punching shear.

3) According to the materials used to construct the circular isolated footing (Reinforcing steel and concrete), the new model is more economical with respect to the model proposed by Luévanos-Rojas [25] and on any other model.

4) The new model occupies less contact surface with the soil compared to the model proposed by Luévanos-Rojas [25]. This results into a smaller volume of soil excavation and therefore generates a greater savings.

5) If the eccentricity increases, greater savings are obtained using the new model (see Table 5).

6) The new model is verified by equilibrium for moment and bending shear.

The suggestions for future research could be

1) Minimum cost design of a circular isolated footing by the new model presented in this document using optimization techniques.

2) When totally cohesive soils (clay soils) and/or totally granular soils (sandy soils) are presented, the pressure diagram is different, because the pressure is not linear as it presented herein.

REFERENCES

[1] J. E. Bowles, *Foundation Analysis and Design*, McGraw-Hill, New York, U.S.A., 2001.

[2] B. M. Das, *Principles of Foundation Engineering*, Cengage Learning, New York, U.S.A., 2007.

[3] A. Luévanos-Rojas, A mathematical model for dimensioning of footings square, *International Review of Civil Engineering*, vol.3, no.4, pp.346-350, 2012.

[4] A. Luévanos-Rojas, A mathematical model for the dimensioning of circular footings, *Far East Journal of Mathematical Sciences*, vol.71, no.2, pp.357-367, 2012.

[5] A. Luévanos-Rojas, A mathematical model for dimensioning of footings rectangular, *ICIC Express Letters, Part B: Applications*, vol.4, no.2, pp.269-274, 2013.

[6] A. Luévanos-Rojas, A new approach for dimensioning of rectangular footings using optimization techniques, *ICIC Express Letters, Part B: Applications*, vol.6, no.11, pp.3141-3146, 2015.

[7] A. Luévanos-Rojas, A comparative study for dimensioning of footings with respect to the contact surface on soil, *International Journal of Innovative Computing, Information and Control*, vol.10, no.4, pp.1313-1326, 2014.

[8] W. L. Filho, R. C. Carvalho, A. L. Christoforo and F. A. R. Lahr, Dimensioning of isolated footing submitted to the under biaxial bending considering the low concrete consumption, *International Journal of Materials Engineering*, vol.7, no.1, pp.1-11, 2017.

[9] S. López-Chavarría, A. Luévanos-Rojas and M. Medina-Elizondo, A mathematical model for dimensioning of square isolated footings using optimization techniques: General case, *International Journal of Innovative Computing, Information and Control*, vol.13, no.1, pp.67-74, 2017.

[10] S. López-Chavarría, A. Luévanos-Rojas and M. Medina-Elizondo, Optimal dimensioning for the corner combined footings, *Advances in Computational Design*, vol.2, no.2, pp.169-183, 2017.

[11] M. Jahanandish, M. Veiskarami and A. Ghahramani, Effect of foundation size and roughness on the bearing capacity factor, Nγ, by stress level-based ZEL method, *Arabian Journal for Science and Engineering*, vol.37, no.7, pp.1817-1831, 2012.

[12] A. Luévanos-Rojas, A new mathematical model for dimensioning of the boundary trapezoidal combined footings, *International Journal of Innovative Computing, Information and Control*, vol.11, no.4, pp.1269-1279, 2015.

[13] A. Luévanos-Rojas, A mathematical model for the dimensioning of combined footings of rectangular shape, *Revista Técnica de la Facultad de Ingeniería Universidad del Zulia*, vol.39, no.1, pp.3-9, 2016.

[14] A. Luévanos-Rojas, S. López-Chavarría and M. Medina-Elizondo, A new model for T-shaped combined footings Part I: Optimal dimensioning, *Geomechanics and Engineering*, vol.14, no.1, pp.51-60, 2018.

[15] G. Aguilera-Mancilla, A. Luévanos-Rojas, S. López-Chavarría and M. Medina-Elizondo, Modeling for the strap combined footings Part I: Optimal dimensioning, *Steel and Composite Structures*, vol.30, no.2, pp.97-108, 2019.

[16] R. Irles-Más and F. Irles-Más, Explicit stresses under rectangular detached footings with biaxial bending, *Informes de la Construcción*, vol.44, no.419, pp.77-90, 1992.

[17] H. M. Algin, Stresses from linearly distributed pressures over rectangular areas, *International Journal Numerical Analytical Methods in Geomechanics*, vol.24, no.8, pp.681-692, 2000.

[18] H. M. Algin, Practical formula for dimensioning a rectangular footing, *Engineering Structures*, vol.29, no.6, pp.1128-1134, 2007.

[19] G. Özmen, Determination of base stresses in rectangular footings under biaxial bending, *Teknik Dergi Digest*, vol.22, no.4, pp.1519-1535, 2011.

[20] J. Bellos and N. P. Bakas, High computational efficiency through generic analytical formulation for linear soil pressure distribution of rigid spread rectangular footings, *Proceedings of the VII European Congress on Computational Methods in Applied Sciences and Engineering*, Crete Island, Greece, 2016.

[21] J. Bellos and N. P. Bakas, Complete analytical solution for linear soil pressure distribution under rigid rectangular spread footings, *International Journal of Geomechanics*, vol.17, no.7, https://doi.org/10.1061/(ASCE)GM.1943-5622.0000874, 2017.

[22] I. Aydogdu, New iterative method to calculate base stress of footings under biaxial bending, *International Journal of Engineering & Applied Sciences (IJEAS)*, vol.8, no.4, pp.40-48, 2016.

[23] K. Girgin, Simplified formulations for the determination of rotational spring constants in rigid spread footings resting on tensionless soil, *Journal of Civil Engineering and Management*, vol.23, no.4, pp.464-474, 2017.

[24] A. Luévanos-Rojas, J. G. Faudoa-Herrera, R. A. Andrade-Vallejo and M. A. Cano-Alvarez, Design of isolated footings of rectangular form using a new model, *International Journal of Innovative Computing, Information and Control*, vol.9, no.10, pp.4001-4021, 2013.

[25] A. Luévanos-Rojas, Design of isolated footings of circular form using a new model, *Structural Engineering and Mechanics*, vol.52, no.4, pp.767-786, 2014.

[26] S. López-Chavarría, A. Luévanos-Rojas and M. Medina-Elizondo, A new mathematical model for design of square isolated footings for general case, *International Journal of Innovative Computing, Information and Control*, vol.13, no.4, pp.1149-1168, 2017.

[27] A. Luévanos-Rojas, Design of boundary combined footings of rectangular shape using a new model, *DYNA Colombia*, vol.81, no.188, pp.199-208, 2014.

[28] A. Luévanos-Rojas, A new model for the design of rectangular combined boundary footings with two restricted opposite sides, *Revista ALCONPAT*, vol.6, no.2, pp.172-187, 2015.

[29] A. Luévanos-Rojas, Design of boundary combined footings of trapezoidal form using a new model, *Structural Engineering and Mechanics*, vol.56, no.5, pp.745-765, 2015.

[30] A. Luévanos-Rojas, S. López-Chavarría and M. Medina-Elizondo, A new model for T-shaped combined footings Part II: Mathematical model for design, *Geomechanics and Engineering*, vol.14, no.1, pp.61-69, 2018.

[31] J. A. Yáñez-Palafox, A. Luévanos-Rojas, S. López-Chavarría and M. Medina-Elizondo, Modeling for the strap combined footings Part II: Mathematical model for design, *Steel and Composite Structures*, vol.30, no.2, pp.109-121, 2019.

[32] A. Luévanos-Rojas, S. López-Chavarría and M. Medina-Elizondo, Optimal design for rectangular isolated footings using the real soil pressure, *Ingeniería e Investigación*, vol.37, no.2, pp.25-33, 2017.

[33] S. López-Chavarría, A. Luévanos-Rojas and M. Medina-Elizondo, Optimal design for the reinforced concrete circular isolated footings, *Advances in Computational Design*, vol.4, no.3, pp.273-294, 2019.

[34] S. Soto-García, A. Luévanos-Rojas, J. D. Barquero-Cabrero, S. López-Chavarría, M. Medina-Elizondo, O. M. Farias-Montemayor and C. Martínez-Aguilar, A new model for the contact surface with soil of circular isolated footings considering that the contact surface works partially under compression, *International Journal of Innovative Computing, Information and Control*, vol.18, no.4, pp.1103-1116, 2022.

[35] T. Nakashima and Y. Hirano, The features of indicator of the environment-related QOL (Quality of Life), *ICIC Express Letters, Part B: Applications*, vol.10, no.7, pp.613-618, 2019.

[36] ACI 318-19 (American Concrete Institute), *Building Code Requirements for Structural Concrete and Commentary*, Committee 318, New York, U.S.A., 2019.

Author Biography

David Samuel Kim-Sánchez received his B.Sc. degree in Industrial Engineering (2004), Master in Administration (2018), and Doctor Candidate in Administration and Senior Management (2021) from the Facultad de Contaduría y Administración of the Universidad Autónoma de Coahuila. He is professor and researcher of the Facultad de Contaduría y Administración, Piedras Negras campus of the Universidad Autónoma de Coahuila since 2018 to date. His research interests are mathematical models applied to Engineering and Administration.

Arnulfo Luévanos-Rojas received his B.Sc. degree in Civil Engineering (1981), Master in Science with Specialization in Structures (1983), Master in Science with Specialization in Planning and Construction of Works (2000), Master in Administration (2004), and Doctor in Engineering with Specialization in Planning Systems and Construction (2009). He was professor and researcher of the Facultad de Ingeniería, Ciencias y Arquitectura, Gomez Palacio Campus of the Universidad Juarez del Estado de Durango from 2006 to 2015, and of the Facultad de Contaduría y Administración, Torreón campus of the Universidad Autónoma de Coahuila since 2015 to date. He has published more than 110 papers in journals indexed in the Web of Science. His research interests are mathematical models applied to Engineering and Administration. He is member of the National System of Researchers of Mexico.

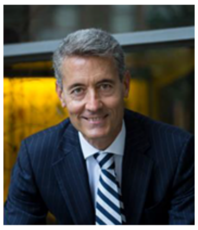

José Daniel Barquero-Cabrero is doctor in the area of Economic, Legal and Social Sciences from the Universidad Internacional de Cataluña, Universidad Camilo José Cela de Madrid, Universitat Oberta de Catalunya, Universidad Autónoma de Coahuila de México and interuniversity by the Universities of Málaga, Huelva, Cádiz y Sevilla. He is also a Chartered Economist no. 13,049. He has been awarded for his contributions to the academic world with the title of doctor honoris causa by universities in America, Europe, Asia and Africa. He was awarded by the Government of Spain, Ministry of Foreign Affairs and Cooperation, the Commendation of the Order of Civil Merit. He was awarded by the European Development Foundation the European Cross in Gold. His research interests are mathematical models applied to Engineering and Administration.

Sandra López-Chavarría received the Master's degree in Administration and Senior Management, and the degree of Doctor in Administration and Senior Management from the Facultad de Contaduría y Administración of the Universidad Autónoma de Coahuila. She is the General Coordinator of the Torreón campus of the Universidad Autónoma de Coahuila. She is professor and researcher for the Facultad de Contaduría y Administración, Torreón campus of the Universidad Autónoma de Coahuila. Her research interests are mathematical models applied to Engineering and Administration. She is member of the National System of Researchers of Mexico.

Manuel Medina-Elizondo received Master in Administration, Master in Management Science and Innovation, Doctor in Administration Sciences from the Universidad Nacional Autónoma de México, and Doctor in Administration from the Universidad de Newport of the State of California, U.S.A. He is current Chairman of the Delegation of Mexico's Superior Council of Doctors and Doctors Honoris Causa. He is professor, researcher, and General Coordinator of Research and Postgraduate of the Facultad de Contaduría y Administración, Torreón campus of the Universidad Autónoma de Coahuila. He has published more than 80 papers, and 15 books. His research interests are mathematical models applied to Engineering and Administration.

Inocencio Luévanos-Soto received B.Sc. degree in Architect (2009), Master in Science with Specialization in Planning and Construction of Works (2012), and Doctor Candidate in Engineering with Specialization in Planning Systems and Construction (2019) from the Universidad Juarez del Estado de Durango. He is professor and researcher of the Facultad de Ingeniería, Ciencias y Arquitectura, Gomez Palacio Campus of the Universidad Juarez del Estado de Durango from since 2010 to date. His research interests are mathematical models applied to Engineering and Architect.